AIAA Aviation
16-20 June 2014, Atlanta, GA
20th AIAA/CEAS Aeroacoustics Conference

Influence of nozzle-exit boundary-layer profile on high-subsonic jets

Christophe Bogey* and **Olivier Marsden†**
Laboratoire de Mécanique des Fluides et d'Acoustique
UMR CNRS 5509, Ecole Centrale de Lyon
69134 Ecully, France

The influence of the nozzle-exit boundary-layer profile on high-subsonic round jets is investigated by performing compressible large-eddy simulations of four jets using low-dissipation numerical schemes. The jets are isothermal, and have a Mach number of 0.9 and a diameter-based Reynolds number of 5×10^4. They originate from a pipe nozzle in which a trip-like forcing is applied. In that way, they exhibit, at the exit section, around 6% of peak turbulence intensity and boundary-layer velocity profiles characterized by a momentum thickness of about 2.8% of the nozzle radius, yielding a Reynolds number around 700, and by shape factors equal to 1.68, 1.77, 2.01 and 2.36. The results from the fourth case with a laminar velocity profile differ significantly from those from the three first cases with transitional profiles, whose accuracy is shown by a grid refinement study. Clear trends are thus identified when the shape of the exit boundary-layer profile changes from laminar to turbulent. Higher azimuthal modes and higher Strouhal numbers are found to predominate, respectively, at the pipe exit close to the wall and early on in the mixing layers. The latter appear to develop more slowly, leading to a longer potential core, and weaker velocity fluctuations are obtained in the shear layers and on the jet axis. Finally, lower noise levels are generated in the acoustic field.

I. Introduction

There has been a considerable amount of work on the effects of jet initial conditions for more than four decades. In particular, a great attention has been paid to the state of the nozzle-exit boundary layer, which may vary from one experiment to another depending on the facility characteristics and on the nozzle diameter and geometry. For instance, the jets are often initially laminar in small-scale experiments, whereas they are initially turbulent in full-scale experiments. In order to make meaningful comparisons, it is thus necessary in the first case to trip the boundary layer in the nozzle to generate turbulent exit conditions, as was the case in the pioneering work of Crow & Champagne.[1]

The differences obtained between initially laminar and initially turbulent jets have been described in a number of papers. It has been shown by Hill *et al.*,[2] Browand & Latigo,[3] Hussain & Zedan[4] and Husain & Hussain,[5] among others, that downstream of the nozzle lip, the turbulence intensity rapidly increases and reaches a peak in the laminar case, whereas it grows monotonically in the turbulent case. Moreover, the jet flow development is found to be faster in the former case than in the latter, leading to a shorter potential core and a higher rate of centerline velocity decay, refer to the data of Hill *et al.*,[2] Raman *et al.*,[6,7] Russ & Strykowski[8] and Xu & Antonia,[9] for example. The impact of the nozzle-exit boundary-layer state is also significant on jet acoustic sources, as pointed out in the review papers by Crighton[10] and Lilley.[11] It has notably been established that initially laminar jets emit more noise than initially turbulent jets, eg in Maestrello & McDaid,[12] Zaman[13,14] and Bridges & Hussain,[15] and that the additional noise can be attributed to the pairings of coherent vortices in the shear layers.

*CNRS Research Scientist, AIAA Senior Member & Associate Fellow, christophe.bogey@ec-lyon.fr
†Assistant Professor at Ecole Centrale de Lyon, olivier.marsden@ec-lyon.fr

The issue of jet initial conditions has recently received renewed attention since Viswanathan[16]'s claim that the jet noise database of Tanna[17] could be contaminated by spurious facility noise. In reply to this, Harper-Bourne[18] suggested that the extra components observed at high frequencies in Tanna[17]'s sound spectra are due to laminar flow conditions at the nozzle exit. This seems to be confirmed by the experimental results obtained by Viswanathan & Clark,[19] Zaman[20] and Karon & Ahuja[21] for jets exhausting from the so-called ASME and conical nozzles of identical exit diameter, differing in internal profile. More high-frequency noise is indeed measured using the ASME nozzle with a nozzle-exit highly disturbed laminar boundary layer than using the conical nozzle with a fully developed boundary layer.

The roles of the different nozzle-exit parameters in the trends reported above are however difficult to distinguish, because these parameters usually vary simultaneously. When the nozzle-exit flow conditions become turbulent, with or without boundary-layer tripping, the shape factor of the boundary-layer profile decreases. This factor, defined as $\mathrm{H} = \delta^*/\delta_\theta$ where δ^* and δ_θ are the boundary-layer displacement and momentum thicknesses, thus takes values around 2.5 for laminar profiles and 1.4 for turbulent profiles. At the same time, the boundary-layer thickness increases, and the peak turbulence intensities u'_e/u_j, where u'_e and u_j are the maximum rms value of velocity fluctuations and the jet velocity, most often grow. In some experiments, similar turbulence levels are obtained, as, for instance, in the work of Morris & Zaman[36] where values of u'_e/u_j equal to 6.7% and 7.5% are found in untripped and tripped jets at a diameter-based Reynolds number $\mathrm{Re}_D = 3 \times 10^5$. It even happens that the velocity fluctuations are larger in laminar nozzle-exit boundary layers than in the turbulent case. Examples of this counterintuitive tendency have been reported by Raman *et al.*[6,7] for tripped/untripped jets and by Zaman[20] who measured values of u'_e/u_j around 11% using the ASME nozzle with a laminar exit boundary layer, but around 7% using the conical nozzle with a turbulent boundary layer. In that case, the effects of the velocity profile and those of the turbulence levels are likely to counteract each other, which may result in some confusion.

On the basis on what precedes, there is clearly still a need to study the influence of the nozzle-exit boundary-layer profile carefully with all other exit parameters held constant. For this, it seems worthwhile to use unsteady compressible simulations, which have made spectacular progress over the last two decades, see in Colonius & Lele,[23] Bailly & Bogey[24] and Wang *et al.*,[25] and now allow us to conduct investigations under controlled conditions. Large-eddy simulations (LES) have for instance been run over the past few years by Bogey *et al.*[26–31] to examine the impact of exit conditions on initially laminar and highly disturbed subsonic round jets. Due to limitations in computing resources, the jets had moderate Reynolds numbers between $\mathrm{Re}_D = 2.5 \times 10^4$ and $\mathrm{Re}_D = 2 \times 10^5$, and exhibited laminar mean velocity profiles at the nozzle exit, which ensured numerical accuracy. First attempts to compute initially turbulent jets were made by Bogey *et al.*[32] and Uzun & Hussaini.[33] However, the grid was too coarse in the former case, while its spatial extent was limited to 4.5 diameters downstream of the nozzle in the latter. More recently, Sandberg *et al.*[34] carried out the simulation of a fully turbulent pipe flow at $\mathrm{Re}_D = 7,500$ exiting into a coflow, and Bühler *et al.*[35] successfully computed a jet at $\mathrm{Re}_D = 18,100$ with turbulent conditions at the exit of a pipe nozzle. None of these studies addresses the question of the mean velocity profile.

In the present work, four isothermal round jets are calculated using LES specifically to investigate the influence of the nozzle-exit boundary-layer profile. The LES are performed on a grid containing 281 million points using low-dissipation finite differences and relaxation filtering as subgrid dissipation. The jets have a Mach number $\mathrm{M} = u_j/c_a = 0.9$ and a Reynolds number $\mathrm{Re}_D = u_j D/\nu = 5 \times 10^4$, where c_a, D and ν are the speed of sound in the ambient medium, the jet diameter and the kinematic molecular viscosity. They originate from a pipe nozzle of radius $r_0 = D/2$ and length $2r_0$, at the inlet of which laminar, transitional or turbulent mean velocity profiles are imposed, and in which a trip-like forcing is employed[27] in order to generate a desired level of turbulent fluctuations. In that way, at the nozzle exit, the boundary-layer profiles have similar momentum thicknesses $\delta_\theta \simeq 0.028 r_0$, but various forms, yielding shape factors H of 1.68, 1.77, 2.01 and 2.36, and the peak turbulence intensities u'_e/u_j are close to 6% in all jets. This set of simulations will allow us to identify the effects due to the exit boundary-layer profile alone. It will then be possible to determine whether the resulting changes are significant, and whether they correspond to those usually encountered when initially laminar jets are tripped, namely a slower flow development, weaker velocity fluctuations and less noise.

The paper is organized as follows. The main characteristics of the different jets and of the simulations, including inflow conditions, numerical methods and computational parameters, are documented in section II. The nozzle-exit flow properties, the mixing-layer and jet flow fields and the jet acoustic fields are described in section III. Concluding remarks are given in section IV. Finally, comparisons between pipe-nozzle inlet veloc-

ity profiles and boundary-layer measurements are shown in appendix A, and results from a grid refinement study are provided in appendix B in order to demonstrate the simulation accuracy.

II. Parameters

In this section, the jet inflow conditions are first presented. The numerical methods and parameters are then briefly reported. In most cases, they are identical to those used in recent jet simulations, which have been thoroughly described in previous references.[27–31] A great amount of information about the boundary-layer tripping procedure, the discretization quality and the LES reliability is moreover available.[27]

A. Jet definition

Four jets, referred to as jetBL, jetT1, jetT2 and jetT3, are considered. They are isothermal, and have a Mach number M = 0.9 and a Reynolds number $\mathrm{Re}_D = 5 \times 10^4$. The ambient temperature and pressure are $T_a = 293$ K and $p_a = 10^5$ Pa. The jets originate at $z = 0$ from a pipe nozzle of radius r_0 and length $2r_0$, whose lip is $0.053r_0$ thick. At the pipe inlet, different axial velocity profiles, whose main parameters are collected in table 1, are imposed. Radial and azimuthal velocities are set to zero, pressure is equal to p_a, and temperature is determined by a Crocco-Busemann relation.

Table 1. Jet inflow parameters: Mach number $\mathrm{M} = u_j/c_a$, Reynolds number $\mathrm{Re}_D = u_j D/\nu_j$, shape factor H, momentum thickness δ_θ and 99% velocity thickness δ_{99} of the boundary-layer profile at the pipe-nozzle inlet, and strength of the trip-like excitation α_{trip} (subscripts j and a denote inflow and ambient conditions).

	M	Re_D	H	δ_θ/r_0	δ_{99}/r_0	α_{trip}
jetBL	0.9	5×10^4	2.55	0.0288	0.202	0.0460
jetT1	0.9	5×10^4	1.88	0.0288	0.215	0.0675
jetT2	0.9	5×10^4	1.52	0.0288	0.254	0.0830
jetT3	0.9	5×10^4	1.40	0.0288	0.278	0.0895

The inlet axial velocity profiles are represented in figure 1(a). In jetBL, the profile is a Blasius laminar boundary-layer profile with a shape factor H = 2.55, given by the Pohlhausen's fourth-order polynomial approximation

$$\frac{u_{inlet}(r)}{u_j} = \begin{cases} \dfrac{(r_0 - r)}{\delta_{BL}} \left[2 - 2 \left(\dfrac{(r_0 - r)}{\delta_{BL}} \right)^2 + \left(\dfrac{r_0 - r}{\delta_{BL}} \right)^3 \right] & \text{if} \quad r \geq r_0 - \delta_{BL} \\ 1 \quad \text{otherwise} \end{cases} \tag{1}$$

In jetT1, jetT2 and jetT3, the inlet profiles are defined as

$$\frac{u_{inlet}(r)}{u_j} = \begin{cases} \left(\sin \left[\dfrac{\pi}{2} \left(\dfrac{r_0 - r}{\delta_{Ti}} \right)^{\beta_i} \right] \right)^{\gamma_i} & \text{if} \quad r \geq r_0 - \delta_{Ti} \\ 1 \quad \text{otherwise} \end{cases} \tag{2}$$

where $i = 1, 2$ and 3 respectively, and the values of the exponents β_i and γ_i are $\beta_1 = 0.464$ and $\gamma_1 = 1.32$, $\beta_2 = 0.423$ and $\gamma_2 = 0.82$, and $\beta_3 = 0.5$ and $\gamma_3 = 0.5$. The T1 and T2 profiles are designed to fit the experimental data obtained by Schubauer & Klebanoff[37] in a flat-plate boundary layer in the region of changeover from laminar to fully turbulent conditions, see the comparisons in Appendix A. They are transitional profiles with shape factors H = 1.88 and 1.52. The T3 profile is the turbulent boundary-layer profile proposed by De Chant,[38] with a shape factor H = 1.40.

The thickness of the inlet boundary-layer profile is set to $\delta_{BL} = 0.25r_0$ in jetBL, $\delta_{T_1} = 1.043\delta_{BL}$ in JetT1, $\delta_{T_2} = 1.328\delta_{BL}$ in JetT2 and $\delta_{T_3} = 1.487\delta_{BL}$ in JetT3, yielding a momentum thickness $\delta_\theta = 0.0288r_0$ and $\mathrm{Re}_\theta = u_j\delta_\theta/\nu = 720$ in all cases. It can be noted that the associated 99% velocity thicknesses vary from $\delta_{99} = 0.202r_0$ in jetBL up to $\delta_{99} = 0.278r_0$ in jetT3.

In order to generate disturbed upstream conditions for the jets, which otherwise would initially contain very weak velocity fluctuations, a forcing is applied to the boundary layers in the pipe. They are thus

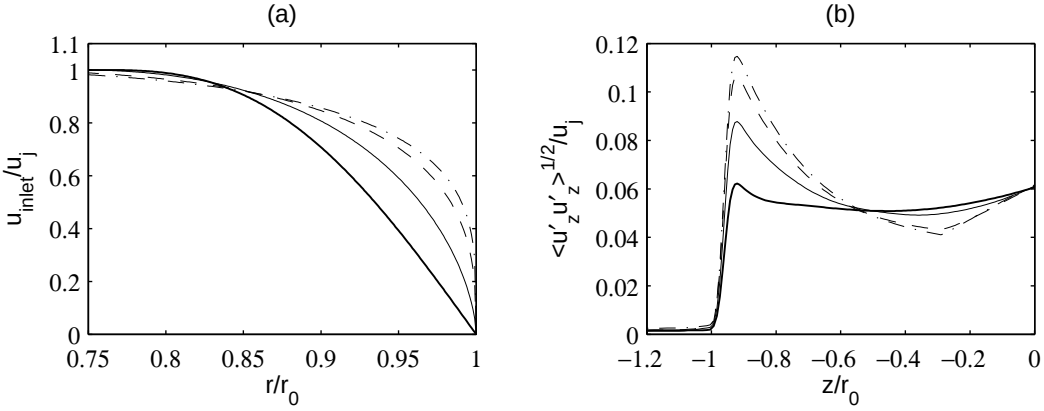

Figure 1. Representation (a) of the axial velocity profile u_{inlet} imposed at the pipe-nozzle inlet and (b) of the peak rms value of axial velocity fluctuations u'_z in the nozzle: ——— jetBL, ——— jetT1, − − − jetT2, − · − · jetT3.

'tripped' as is usually done in laboratory experiments for boundary layers over a flat plate or in jet nozzle, eg in Klebanoff & Diehl[39] and Crow & Champagne.[1] The choice a tripping device is arbitrary, and different devices may lead to disparities between results, which have been discussed for a long time.[39–44] Therefore, the same forcing procedure, detailed in the appendix A of Bogey *et al.*,[27] is implemented in the present jets. It consists in adding random low-level vortical disturbances decorrelated in the azimuthal direction in the boundary layers, at $z = -0.95r_0$ and at a radial position based on δ_{BL} in all cases. However, the forcing magnitudes are not identical. They have been fixed after preliminary tests to obtain peak nozzle-exit turbulence intensities u'_e/u_j around 6%. This level is comparable to those measured by Zaman[20] for initially turbulent jets just downstream of a conical nozzle. As indicated in table 1, the value of the coefficient α_{trip} specifying the forcing strength is set to 0.046, 0.0675, 0.083 and 0.095 in jetBL, jetT1, jetT2 and jetT3. Consequently, the lower the inlet boundary-layer shape factor, the higher the amplitude of the trip-like excitation necessary to reach $u'_e/u_j \simeq 6\%$. This is illustrated in figure 1(b) showing the variations of the maximum rms value of axial velocity fluctuations in the pipe. Finally, pressure fluctuations of maximum amplitude 200 Pa random in both space and time are added in the shear layers between $z = 0.25r_0$ and $z = 4r_0$ from $t = 0$ up to non-dimensional time $t = 12.5r_0/u_j$, in order to speed up the initial transitory period.

B. LES procedure and numerical methods

The LES are carried out using a solver of the three-dimensional filtered compressible Navier-Stokes equations in cylindrical coordinates (r, θ, z) based on low-dissipation and low-dispersion explicit schemes. The axis singularity is taken into account by the method of Mohseni & Colonius.[45] In order to alleviate the time-step restriction near the cylindrical origin, the derivatives in the azimuthal direction around the axis are calculated at coarser resolutions than permitted by the grid.[46] Fourth-order eleven-point centered finite differences are used for spatial discretization, and a second-order six-stage Runge-Kutta algorithm is implemented for time integration.[47] A sixth-order eleven-point centered filter[48] is applied explicitly to the flow variables every time step. Non-centered finite differences and filters are also used near the pipe walls and the grid boundaries.[26,49] The radiation conditions of Tam & Dong[50] are applied at all boundaries, with the addition at the outflow of a sponge zone combining grid stretching and Laplacian filtering.[51]

The explicit filtering is employed to remove grid-to-grid oscillations, but also as a subgrid high-order dissipation model in order to relax turbulent energy from scales at wave numbers close to the grid cut-off wave number while leaving larger scales mostly unaffected.[52–55] With this in mind, the reliability of the LES fields obtained for a jet at $\mathrm{Re}_D = 10^5$ has been assessed in Bogey *et al.*[27] based on the tranfer functions associated with molecular viscosity, relaxation filtering and time integration. Viscosity was shown to be the dominant dissipation mechanism for scales discretized at least by seven points per wavelength. The physics of the larger turbulent structures is therefore unlikely to be governed by numerical or subgrid-modeling dissipation. This allows the effective flow Reynolds number not to be artificially decreased, and viscosity effects to be captured, as was the case in Bogey *et al.*[30] for jets at Re_D between 2.5×10^4 and 2×10^5. These remarks certainly equally hold true for the present LES dealing with jets at $\mathrm{Re}_D = 5 \times 10^4$.

C. Simulation parameters

As reported in table 2, the LES grid contains $n_r \times n_\theta \times n_z = 273 \times 1024 \times 107 = 281$ million points. For $z \leq 25r_0$ and $r \leq 6.5r_0$, it is identical to that used in recent simulations[27–31] for subsonic jets with laminar boundary-layer profiles. There are 169 points along the pipe nozzle between $z = -2r_0$ and $z = 0$, 77 points within the jet radius, and 41 points between $r = r0 - \delta_{BL} = 0.75r_0$ and $r = r_0$. The physical domain, excluding the eighty-point outflow sponge zone, extends axially down to $L_z = 28r_0$, and radially out to $L_r = 11r_0$.

Table 2. Simulation parameters: numbers of grid points n_r, n_θ and n_z, mesh spacings Δr at $r = r_0$, $r_0\Delta\theta$, and Δz at $z = 0$, extents L_r and L_z of the physical domain, radial position r_c of the far-field extrapolation surface, number of time steps n_{it} and time duration T ($^*n_{it}$ =142,500 and $Tu_j/r_0 = 325$ for jetT3).

$n_r \times n_\theta \times n_z$	$\Delta r/r_0$	$r_0\Delta\theta/r_0$	$\Delta z/r_0$	L_r, L_z	r_c/r_0	n_{it}	Tu_j/r_0
$273 \times 1024 \times 1007$	0.36%	0.61%	0.72%	$11r_0, 28r_0$	7.5	164,000*	375*

The mesh spacing is uniform in the azimuthal direction, with $r_0\Delta\theta = 0.0061r_0$. In the axial direction, the mesh spacing is minimum between $z = -r_0$ and $z = 0$, with $\Delta z = 0.0072r_0$. It increases upstream of $z = -r_0$, but also downstream of the nozzle at stretching rates lower than 1% allowing to reach $\Delta z = 0.065r_0$ between $z = 13.3r_0$ and $z = L_z = 28r_0$. In the radial direction, the mesh spacing is minimum around $r = r_0$, with $\Delta r = 0.0036r_0$. It is equal to $\Delta r = 0.292r_0$ close to the jet axis, to $\Delta r = 0.081r_0$ between $r = 3r_0$ and $r = 8.75r_0$, and to $\Delta r = 0.176r_0$ at $r = L_r = 11r_0$. Further details regarding the mesh spacings can be found in previous papers.[27,29]

The grid quality has been assessed in Bogey *et al.*[27] and in Bogey & Marsden[31] for Mach number 0.9 jets with laminar nozzle-exit boundary-layer profiles. In the first case, for a jet at $\mathrm{Re}_D = 10^5$ with $\delta_{BL} = 0.15r_0$ and $u'_e/u_j = 9\%$, the ratios between the integral length scales of the axial velocity fluctuations and the mesh spacings on the nozzle-lip line were shown to fall between 4 and 10. The properties of the jet initial turbulence and of the shear-layer flow fields were also proved to be practically grid converged. In the second case, for jets at Re_D around 5×10^4 with $0.09r_0 \leq \delta_{BL} \leq 0.42r_0$, $\mathrm{Re}_\theta = 480$ and $u'_e/u_j = 9\%$, the solutions obtained downstream of the nozzle were found to superpose using a normalization by the exit momentum thickness, supporting their convergence with respect to the grid. Based on these results, there is little doubt that in this work, the grid resolution is appropriate for jetBL with $\mathrm{Re}_D = 5 \times 10^4$, $\delta_{BL} = 0.25r_0$ and $u'_e/u_j = 6\%$, exhibiting laminar boundary-layer profiles.

For jetT1, jetT2 and jetT3 with transitional or turbulent boundary-layer profiles, the suitability of the grid is not obvious at first sight. The near-wall mesh spacings in the pipe expressed in wall units based on the wall friction velocity at the nozzle exit are such that $\Delta r^+ \leq 3$, $(r_0\Delta\theta)^+ \leq 5.1$ and $\Delta z^+ \leq 6$, see the exact values in table 3. The azimuthal and axial mesh spacings are therefore sufficient, because they meet the requirements needed to compute turbulent wall-bounded flows accurately, using direct numerical simulation as in Kim *et al.*[56] and Spalart[57] for instance, or using LES involving relaxation filtering as in Gloerfelt & Berland[58] and Kremer & Bogey.[55] For the wall-normal spacing, a grid convergence study has been conducted using a finer grid. For $z \leq 4r_0$, this grid is identical to the first grid in the directions θ and z, but differs in the radial direction with $\Delta r/r_0 = 0.18\%$ instead of $\Delta r/r_0 = 0.36\%$ at $r = r_0$. In the additional LES, moreover, the tripping procedure is exactly the same as in the LES using the reference grid, and the time step is twice as small because of the CFL stability condition, leading to an application of the relaxation filtering that is twice as frequent. The flow fields obtained using the two grids at the nozzle exit and in the mixing layers developing further downstream have very similar features, as illustrated in Appendix B for jetT2. This demonstrates that the LES solutions do not depend significantly on the radial mesh spacing at $r = r_0$ or on the relaxation filtering.

The simulation time, given in table 2, is equal to $375r_0/u_j$ for jetBL, jetT1, jetT2, and to $325r_0/u_j$ for jetT3 in order to save computational time. After the initial transitory period, density, velocity components and pressure are recorded from time $t = 100r_0/u_j$ onwards, on the jet axis and on two surfaces at $r = r_0$ and $r = r_c = 7.5r_0$, at a sampling frequency allowing the computation of spectra up to a Strouhal number $\mathrm{St}_D = fD/u_j = 20$, where f is the time frequency. The cylindrical surface surrounding the jets is located at $r = 7.5r_0$, in a region where the radial mesh spacing yields a Strouhal number $\mathrm{St}_D = 6.9$ for an acoustic wave discretized by four points per wavelength. In the azimuthal direction, every fourth grid point is stored, allowing data post-processing to be performed up to the azimuthal mode $n_\theta = 128$, where n_θ is the dimensionless azimuthal wave number such that $n_\theta = k_\theta r$. The velocity spectra are evaluated from

Table 3. Near-wall mesh spacings Δr, $r_0\Delta\theta$ and Δz given in wall units based on the wall friction velocity at the nozzle exit.

	Δr^+	$(r_0\Delta\theta)^+$	Δz^+
JetBL	1.4	2.4	2.8
JetT1	2.2	3.7	4.4
JetT2	2.8	4.7	5.6
JetT3	3.0	5.1	6.0

overlapping samples of duration $27.4r_0/u_j$. The flow statistics are determined from $t = 175r_0/u_j$ onwards, and they are averaged in the azimuthal direction. They can be considered to be well converged in view of the results obtained at intermediary stages of the LES for $t \geq 300r_0/u_j$.

The simulations have run using an OpenMP-based in-house solver, on 32 processors of IBM Power7 and x3750M4 computers. A total number of about 400,000 CPU hours have been consumed, for 70 GB of memory required in each case.

D. Far-field extrapolation

The LES near fields of jetBL, jetT1 and jetT2 have been propagated to the acoustic far field by solving the isentropic linearized Euler equations (ILEE) in cylindrical coordinates.[59] This does not appear necessary for jetT3, because of the very strong resemblance between the flow fields of jetT2 and jetT3, which will be shown in sections III.B and III.C. The extrapolation is performed from fluctuating velocities and pressure recorded in the LES on a surface at $r = 7.5r_0$ as mentioned above. These data are interpolated onto a cylindrical surface discretized by an axial mesh spacing of $\Delta z = 0.065r_0$. They are then imposed at the bottom boundary of the grid on which the ILEE are solved using the same numerical methods as in the LES. This grid contains $845 \times 256 \times 1155$ points, and extends axially from $z = -16.6r_0$ to $58.2r_0$ and radially up to $r = 62.4r_0$. The grid spacings are uniform with $\Delta r = \Delta z = 0.065r_0$, yielding $\mathrm{St}_D = 8.6$ for an acoustic wave at four points per wavelength. After a propagation time $t \simeq 60r_0/u_j$, pressure is recorded around the jets at a distance of $60r_0$ from $z = r = 0$, where far-field acoustic conditions are expected to apply according to the experiments of Ahuja *et al.*,[60] during a period of $250r_0/u_j$. Pressure spectra are evaluated using overlapping samples of duration $38r_0/u_j$, and they are averaged in the azimuthal direction.

III. Results

A. Nozzle-exit conditions

The profiles of mean and rms axial velocities calculated at the nozzle exit are presented in figures 2(a-b), and the main exit flow parameters are provided in table 4. As intended, the mean velocity profiles differ significantly in figure 2(a), leading to the shape factors H = 2.36, 2.01, 1.77 and 1.68. The boundary-layer momentum thicknesses δ_θ are all close to a value of $0.028r_0$, yielding $\mathrm{Re}_\theta \simeq 700$, whereas the 99% velocity thicknesses δ_{99} and the vorticity thicknesses δ_ω vary, with the former increasing and the latter decreasing as the velocity profile becomes turbulent. The profile in jetBL therefore corresponds to a laminar profile, and, given that $\mathrm{H} \simeq 1.45$ is obtained[41,42,57,61] for fully developed boundary layers at $\mathrm{Re}_\theta = 700$, the profiles in jetT1, jetT2 and jetT3 are transitional. The radial distributions of axial turbulent intensities also change in figure 2(b), with a peak moving nearer to the wall from the position $r_e = 0.94r_0$ in jetBL nearly up to $r_e = 0.98r_0$ in jetT3. A peak value u'_e/u_j of about 6.1% is however reached in all cases. With respect to the parameters of the inlet boundary layers in table 1, small differences can be noted, due to the flow development in the pipe over the short distance between the forcing at $z = -0.95r_0$ and the exit at $z = 0$. The boundary layer has a lower shape factor and a larger momentum thickness at the exit than at the pipe inlet in jetBL, whereas the opposite trends are observed in the three other jets. Finally, it can be mentioned that in the experiments of Zaman,[20] $\mathrm{Re}_\theta = 920$ and $u'_e/u_j = 6.4\%$ are found just downstream of a conical nozzle for an initially turbulent jet at $\mathrm{Re}_D = 1.9 \times 10^5$, both of which are relatively similar to the values specified in the present jets.

The properties of the jet initial disturbances are examined by computing spectra of axial velocity fluctuations at the nozzle exit. The spectra estimated at the position $r = r_e$ of the turbulence intensity peak

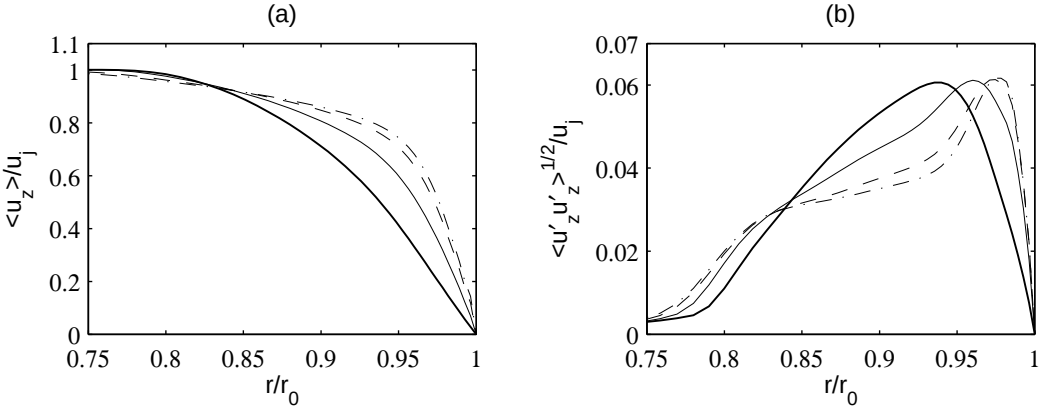

Figure 2. Radial profiles at the nozzle exit (a) of mean axial velocity $< u_z >$ and (b) of the rms values of axial velocity fluctuations u'_z: ——— jetBL, ——— jetT1, − − − jetT2, − · − · jetT3.

Table 4. Nozzle-exit parameters: shape factor H, momentum thickness δ_θ, 99% velocity thickness δ_{99} and vorticity thickness δ_ω of the boundary-layer profile, Reynolds number $\mathrm{Re}_\theta = u_j\delta_\theta/\nu$, value u'_e/u_j and radial position r_e of peak axial turbulence intensity, and peak azimuthal mode n_θ at $r = r_e$.

	H	δ_θ/r_0	δ_{99}/r_0	δ_ω/r_0	Re_θ	u'_e/u_j	r_e/r_0	n_θ
JetBL	2.36	0.0297	0.208	0.117	742	6.07%	0.940	40
JetT1	2.01	0.0284	0.217	0.061	709	6.13%	0.960	45
JetT2	1.77	0.0276	0.244	0.041	691	6.14%	0.975	61
JetT3	1.68	0.0275	0.264	0.036	687	6.16%	0.978	61

are represented as a function of the Strouhal number St_D in figure 3(a), and of the azimuthal mode n_θ in figure 3(b). Their shapes are roughly the same in the four cases, and correspond, as was discussed in a specific note[28] on that matter, to the spectral shapes encountered for turbulent wall-bounded flows because of the presence of large-scale elongated structures. As the boundary-layer profile changes from laminar to turbulent, the magnitude of the low-frequency components at $\mathrm{St}_D < 0.4$ appears to strengthen slightly in figure 3(a). Most obviously, the dominant components in figure 3(b) shift towards higher modes, resulting in peaks at $n_\theta = 40$ in jetBL, $n_\theta = 45$ in jetT1 and $n_\theta = 61$ in jetT2 and jetT3, as reported in table 4. At the location of peak turbulence intensity, the turbulent structures are thus spaced out by $\lambda_\theta = 0.15r_0$, $\lambda_\theta = 0.13r_0$ and $\lambda_\theta = 0.10r_0$, respectively. This modification of their spatial arrangement in the azimuthal direction can be related to the increase of the velocity gradient near the wall.

The spectra evaluated further from the wall at $r = 0.835r_0$, where the rms values of axial velocity fluctuations are of about $0.03u_j$ in the four jets, are depicted in figures 4(a-b). Overall, they look like the near-wall velocity spectra shown above. Two important differences can however be noticed. First, a significant amount of energy is contained by the components centered around a Strouhal numbers $\mathrm{St}_D = 3.2$ in figure 4(a), whereas a rapid collapse is observed for $\mathrm{St}_D \geq 1$ in figure 3(a). Second, the dominant mode in the azimuthal direction is $n_\theta = 40$ in all cases in figure 4(b), whereas it increases with decreasing the boundary-layer shape factor in figure 3(b). The turbulent structures therefore organize differently near the wall and further away, that is, in the inner and the outer flow regions, as expected.[62] In the latter region, furthermore, they turn out not to depend much on the form of the velocity profile.

B. Shear-layer development

Snapshots of the vorticity norm obtained for jetBL, jetT1 and jetT2 down to $z = 3r_0$ and $z = 10r_0$ are represented in figures 5 and 6, respectively. As the nozzle-exit boundary-layer profile switches from laminar to turbulent, higher levels of vorticity are found in figure 5 immediately downstream of the nozzle lip, unsurprisingly given the sharper velocity profiles of figure 1(a). In that region, structures elongated in the streamwise direction, typical of wall-bounded flows, can be seen. The shear layers seem to roll up around $z = 1.5r_0$, and then exhibit large-scale structures resembling the coherent structures revealed by the flow

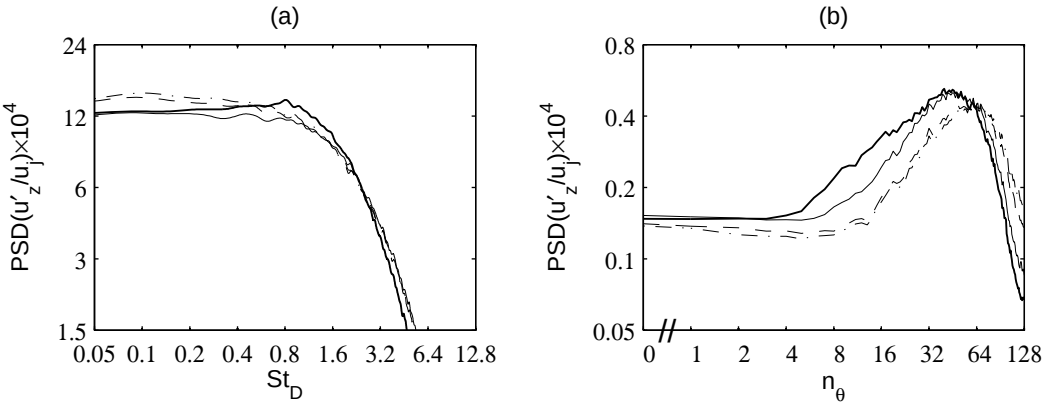

Figure 3. Power spectral densities (PSD) of axial velocity fluctuations u'_z obtained at the nozzle exit at the position $r = r_e$ of peak axial turbulence intensity, as functions (a) of Strouhal number $\mathrm{St}_D = fD/u_j$ and (b) of azimuthal mode n_θ: ——— jetBL, ——— jetT1, – – – jetT2, – · – · jetT3.

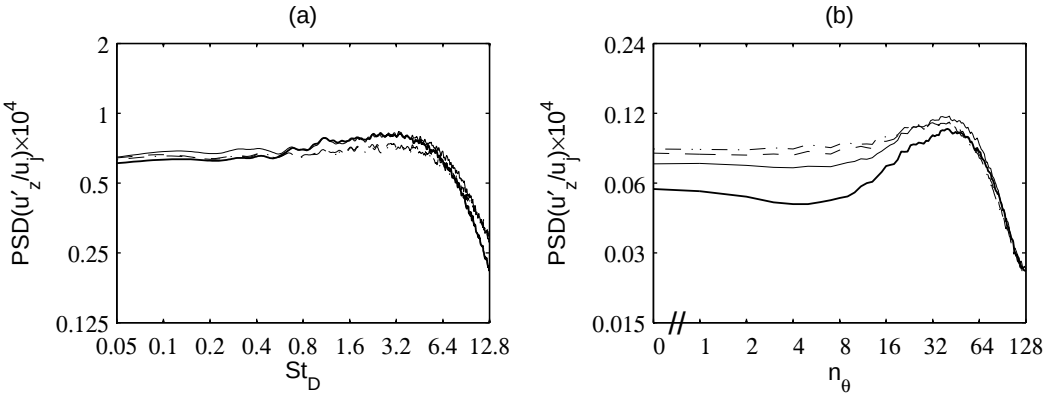

Figure 4. Power spectral densities (PSD) of axial velocity fluctuations u'_z obtained at the nozzle exit at $r = 0.835r_0$, as functions (a) of Strouhal number St_D and (b) of azimuthal mode n_θ: ——— jetBL, ——— jetT1, – – – jetT2, – · – · jetT3.

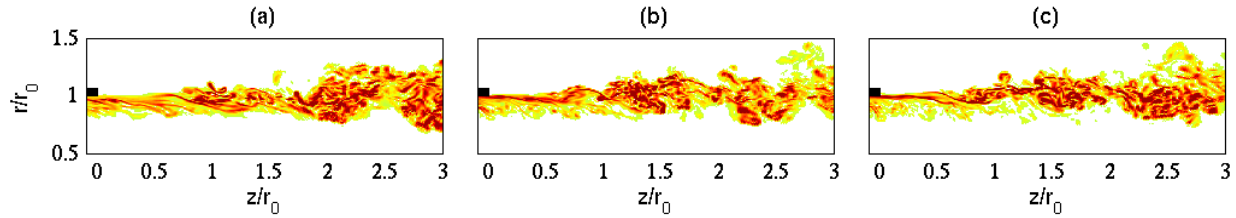

Figure 5. Snapshots in the (z, r) plane of vorticity norm $|\omega|$ for (a) jetBL, (b) jetT1 and (c) jetT2. The color scale ranges up to the level of $18u_j/r_0$,

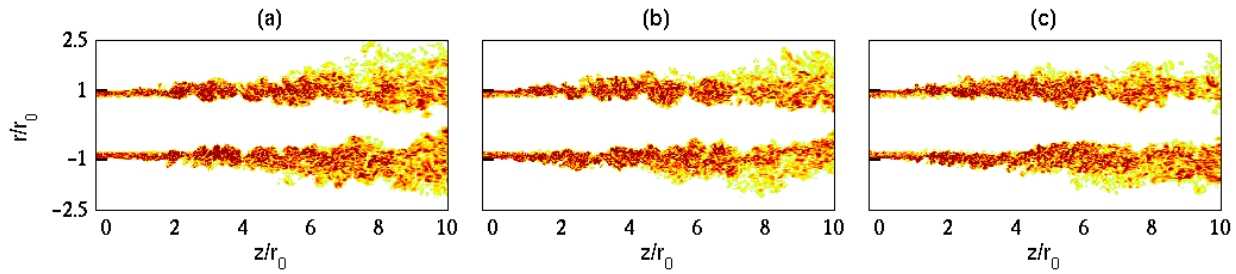

Figure 6. Snapshots in the (z, r) plane of vorticity norm $|\omega|$ for (a) jetBL, (b) jetT1 and (c) jetT2. The color scale ranges up to the level of $9.6u_j/r_0$,

visualizations of Brown & Roshko.[63] Further downstream, in figure 6, they appear to be fully developed for $z \geq 5r_0$, where they may spread more rapidly in jetBL than in the two other jets.

The variations over $0 \leq z \leq 10r_0$ of the momentum thickness δ_θ and of the spreading rate $\mathrm{d}\delta_\theta/\mathrm{d}z$ of the mixing layers are presented in figures 7(a-b). According to figure 7(a), the shear layers develop first more rapidly and then, in a second stage, more slowly in the jets with nozzle-exit transitional velocity profiles than in the jet with a laminar profile. As a result, the curves obtained for the spreading rate vary significantly in figure 7(b). In jetBL, it increases steadily with the axial distance to reach values higher than $\mathrm{d}\delta_\theta/\mathrm{d}z = 0.28$ between $z = 4r_0$ and $z = 10r_0$. In the other jets, on the contrary, a peak value, equal to 0.28 in jetT1, 0.31 in jetT2 and 0.32 in jetT3, is achieved at $z \simeq r_0$, and spreading rates lower than 0.24 are found for $z \geq 4r_0$. Note that the differences are strong between jetBL and jetT1, namely between the laminar case with H = 2.36 and the transitional case with H = 2.01, but that they are rather weak between the three cases with $1.68 \leq \mathrm{H} \leq 2.01$.

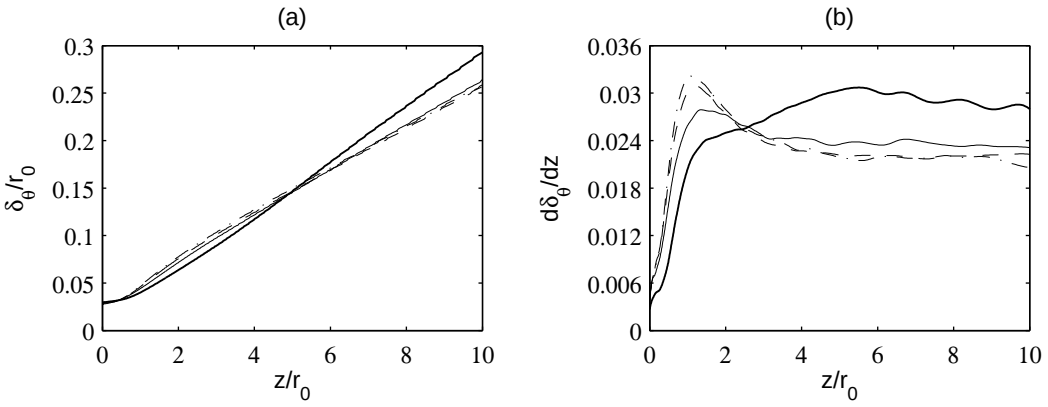

Figure 7. Variations (a) of shear-layer momentum thickness δ_θ and (b) of spreading rate $\mathrm{d}\delta_\theta/\mathrm{d}z$: ——— jetBL, ——— jetT1, − − − jetT2, − · − · jetT3.

The variations over $0 \leq z \leq 14r_0$ of the peak rms values of axial and radial velocity fluctuations are displayed in figures 8(a-b). They follow trends which are similar to those described above for the mixing-layer spreading rate. As the boundary-layer shape factor decreases, the turbulence intensities progressively grow just downstream of the nozzle to form a small hump around $z = r_0$. Most remarkably, they are strongly reduced from $z = 2.2r_0$ down to $z = 14r_0$, that is, from a position relatively close to the nozzle exit down to approximately the end of the jet potential core. At $z = 8r_0$, for instance, the levels are of 16.8%, 15.1%, 14.7% and 14.7% for u'_z, and of 12.3%, 11%, 10.7% and 10.6% for u'_r, see also in table 5 for the maximum turbulence intensities in the jets.

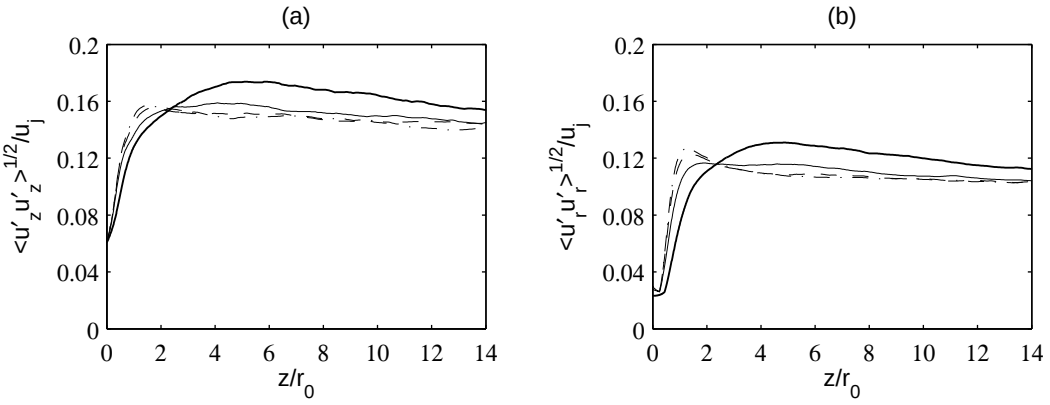

Figure 8. Variations of the peak rms values of (a) axial and (b) radial velocity fluctuations u'_z and u'_r: ——— jetBL, ——— jetT1, − − − jetT2, − · − · jetT3.

Comparing the simulation results with measurements is not easy, because it requires identical upstream flow conditions. It can however be mentioned that in the similarity region of an axisymmetric mixing layer,

Table 5. Peak turbulence intensities in the jets, and Strouhal numbers St_D, $St_\theta = f\delta_\theta(z=0)/u_j$ and $St_\omega = f\delta_\omega(z=0)/u_j$ given by the peak frequency in the spectra of radial velocity fluctuations at $z = r_0$ and $r = r_0$.

	$<u_z'^2>^{1/2}/u_j$	$<u_r'^2>^{1/2}/u_j$	$<u_\theta'^2>^{1/2}/u_j$	$<u_r'u_z'>^{1/2}/u_j$	St_D	St_θ	St_ω
jetBL	17.4%	13.1%	14.5%	10.6%	1.11	0.0165	0.0649
jetT1	15.9%	11.7%	13.5%	9.6%	1.40	0.0199	0.0428
jetT2	15.5%	12.3%	14.0%	9.9%	1.91	0.0264	0.0395
jetT3	15.7%	12.7%	14.0%	9.9%	1.94	0.0267	0.0352

initially with $Re_\theta = 349$, $u'_e/u_j = 6.18\%$ and H = 2.47, Hussain & Zedan[4] obtained a spreading rate of 0.0294 and a peak axial turbulence intensity of 16.7%, which are both comparable to the values reached between $z = 6r_0$ and $z = 10r_0$ in jetBL. Moreover, the changes undergone by the present jet mixing layers as the nozzle-exit velocity profile deviates from a laminar profile, namely a slower growth and weaker velocity fluctuations, correspond to those observed experimentally when initially laminar shear layers are tripped and become initially turbulent, eg in Hill *et al.*,[2] Browand & Latigo[3] and Husain & Hussain.[5] They are also very similar to the changes induced just by increasing the exit turbulence levels, which have been investigated by Hussain & Zedan[64] and Bogey *et al.*[29]

Spectra of radial velocity fluctuations are calculated at $r = r_0$ on the lip line at the two axial locations $z = r_0$ and $z = 8r_0$. They are presented in figures 9(a-b) as a function of the Strouhal number St_D. At the first location, in figure 9(a), an instability-like component is found to emerge in all cases, at a Strouhal number rising as the nozzle-exit velocity profile becomes turbulent. This component is centered around $St_D = 1.11$ in jetBL, 1.40 in jetT1, 1.91 in jetT2 and 1.94 in jetT3, yielding Strouhal numbers based on the exit momentum thickness $St_\theta = 0.0165$, 0.0199, 0.0264 and 0.0267, as reported in table 5. Therefore, the peak frequency obtained for the jet with a laminar boundary-layer profile falls within the range of frequencies predominating early on in initially laminar mixing layers according to linear stability analyses[65] and experiments.[66] For the jets with transitional profiles, it moves out of this range. The shift towards higher frequencies can be attributed to the increase of the velocity gradient. It is then tempting to scale the peak frequencies with the vorticity thickness, which is the maximum-slope thickness of the velocity profile. Unfortunately, it fails since the Strouhal number based on the nozzle-exit vorticity thickness varies from $St_\omega = 0.0649$ in jetBL down to $St_\omega = 0.0352$ in jetT3, refer to table 5.

Further downstream at $z = 8r_0$, in figure 9(b), the radial velocity spectra display similar broadband shapes but different amplitudes. More precisely, the spectra for the jets with initial transitional velocity profiles are close to each other, and show lower levels compared to the spectrum for the jet with a laminar profile. The decrease is especially pronounced for Strouhal numbers $St_D \leq 0.4$, but is more limited at higher frequencies.

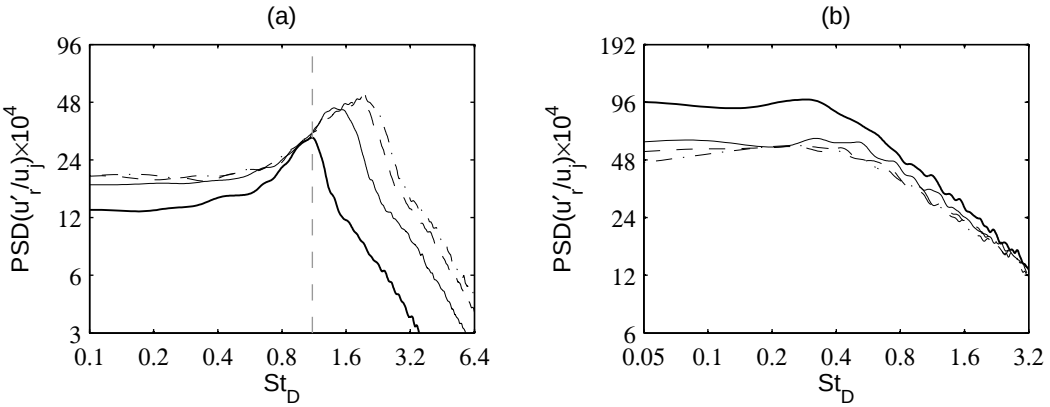

Figure 9. Power spectral densities (PSD) of radial velocity fluctuations u'_r (a) at $z = r_0$ and $r = r_0$ and (b) at $z = 8r_0$ and $r = r_0$, as functions of St_D: ——— jetBL, ——— jetT1, − − − jetT2, − · − · jetT3; – – – frequency given by $St_\theta = f\delta_\theta/u_j = 0.0165$ for $\delta_\theta = 0.0297r_0$.

C. Jet development

Snapshots of the vorticity norm obtained down to $z = 25r_0$ for jetBL, jetT1 and jetT2 are represented in figure 10. With decreasing the shape factor of the nozzle-exit boundary layer, the jet mixing layers visibly merge later, which is consistent with the reduction in shear-layer spreading rate noted in the previous section. Compare for instance figures 10(a) and 10(c): the end of the potential core is around $z = 13r_0$ for jetBL with H = 2.36, but around $z = 16r_0$ for jetT2 with H = 1.77.

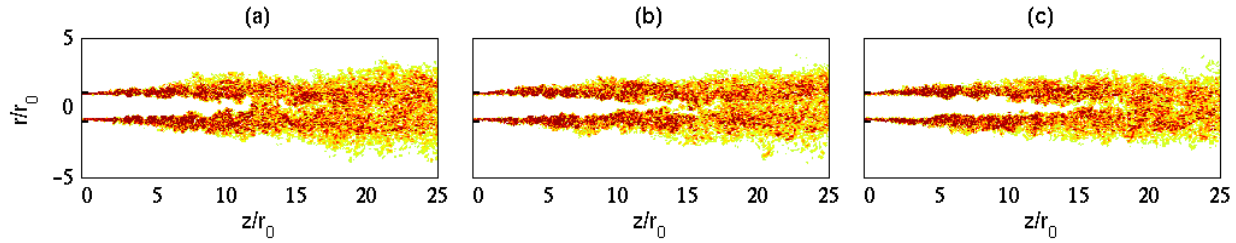

Figure 10. Snapshots in the (z, r) plane of vorticity norm $|\omega|$ for (a) jetBL, (b) jetT1 and (c) jetT2. The color scale ranges up to the level of $5.5u_j/r_0$,

The variations of the centerline mean axial velocity u_c and of the jet half-width $\delta_{0.5}$, defined as the radial distance where $< u_z >= u_c/2$, are presented in figures 11(a-b). As the nozzle-exit boundary-layer profile changes from laminar to turbulent, the jet flow develops more slowly. This leads to potential cores ending at $z_c = 12.5r_0$ in jetBL, $z_c = 15.2r_0$ in jetT1, and $z_c \simeq 16r_0$ in jetT2 and jetT3, as indicated in table 6. Downstream of the potential core, the centerline velocity decay and the jet spreading then appear to occur at similar rates in the four jets.

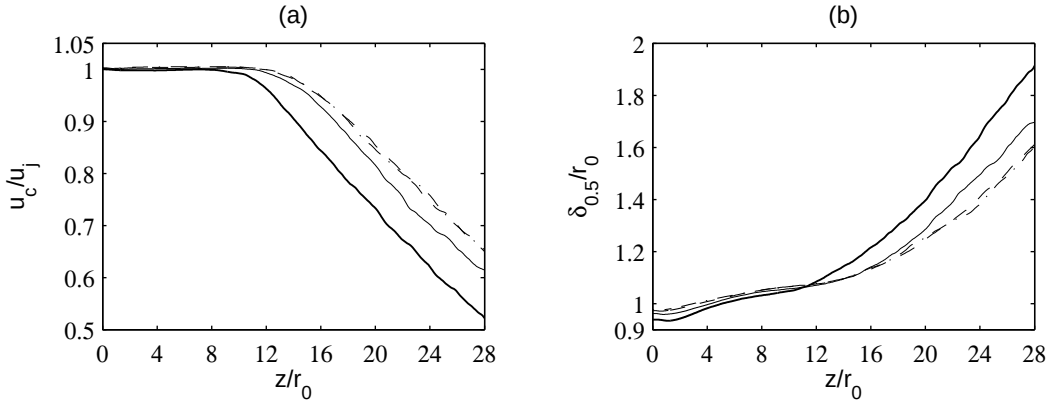

Figure 11. Variations (a) of centerline mean axial velocity u_c and (b) of jet velocity half-width $\delta_{0.5}$: ——— jetBL, ——— jetT1, − − − jetT2, − · − · jetT3.

Table 6. Axial position of the end of the potential core z_c, where $u_c(z_c) = 0.95u_j$, and peak rms values of velocity fluctuations u'_z and u'_r on the jet axis.

	z_c/r_0	$<u'^2_z>^{1/2}/u_j$	$<u'^2_r>^{1/2}/u_j$
JetBL	12.5	12.8%	9.7%
JetT1	15.2	11.5%	9.6%
JetT2	16.0	11.5%	8.9%
JetT3	15.8	11.7%	9.1%

The variations of the centerline rms values of axial and radial velocity fluctuations are shown in figures 12(a-b). The peak turbulence intensities are reached around $z = 16r_0$ in jetBL and $z = 24r_0$ in the three other jets, as expected given the delay in jet flow development reported above. Relative to the end of the potential core, the peaks are however located at $z \simeq z_c + 4r_0$ in the first case, but at $z \simeq z_c + 8r_0$ in the others. Moreover, the maximum values decrease appreciably for velocity u'_z, from 12.8% in jetBL down

to about 11.5% in the other cases, and slightly for velocity u'_r, see in table 6. Here again, the differences are strong between jetBL and jetT1, but quite weak between the three jets with transitional boundary-layer profiles.

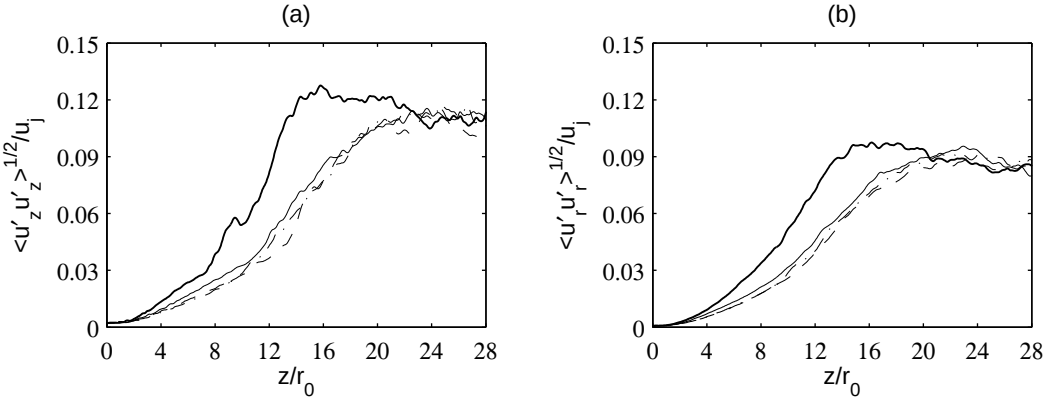

Figure 12. Variations of the centerline rms values of (a) axial and (b) radial velocity fluctuations u'_z and u'_r: ——— jetBL, ——— jetT1, − − − jetT2, − · − · jetT3.

The changes observed between the jets with laminar and transitional exit velocity profiles are comparable to those obtained experimentally between untripped and tripped jets in Raman *et al.*[6,7] and Russ & Strykowski,[8] for example, as well as to those happening when only the initial fluctuation level increases, which are illustrated in Bogey *et al.*[29] Raman *et al.*[6] considered in particular tripped and untripped jets at a Mach number M = 0.3 and a Reynolds number $\mathrm{Re}_D = 6\times10^5$ with nozzle-exit boundary-layer shape factors H ≃ 1.55 and 1.80, respectively, and turbulence intensities close to $u'_e/u_j = 7\%$. The flow development in the tripped jets is shifted by about $2r_0$ in the downstream direction with respect to the untripped jet, which is in line with the present results. The peak turbulence intensities on the centerline are similar, and are located at $z \simeq z_c + 8r_0$ in all cases, which however differs from what is found in figure 12. The reason for this may be that the exit boundary layer of the untripped jet of Raman *et al.*[6] is not laminar but transitional, as suggested by its shape factor H = 1.80. This may also be due[31] to the comparatively large boundary-layer thickness $\delta_\theta \simeq 0.028r_0$ in the simulations, which has been chosen to ensure numerical accuracy.

D. Acoustic fields

Snapshots of the near pressure fields obtained directly by LES for jetBL, jetT1 and jetT2 are provided in figure 13. At first sight, they do not look very different from each other. The magnitude of the acoustic waves seems however to diminish as the jet initial velocity profile transitions from laminar to turbulent. This trend is most noticeable for the waves propagating in the upstream and sideline directions on the left side of figures 13(a) and 13(b).

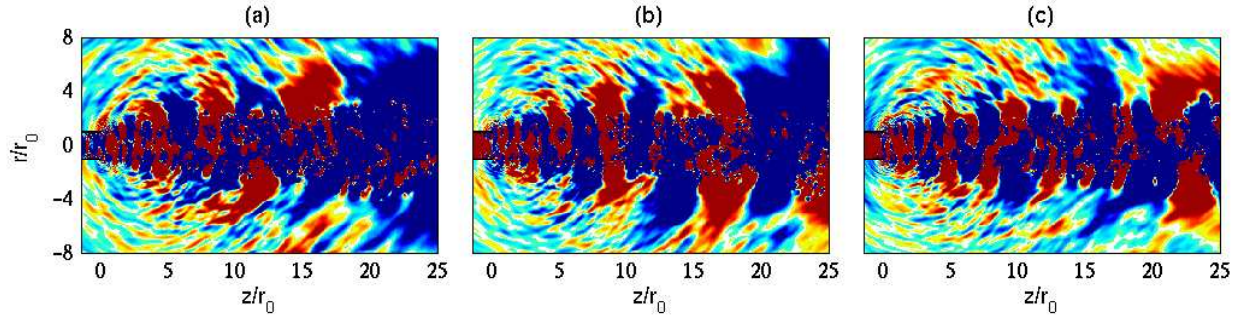

Figure 13. Snapshots in the (z, r) plane of pressure fluctuations $p - p_a$ for (a) jetBL, (b) jetT1 and (c) jetT2. The color scale ranges from −70 to 70 Pa.

Far-field characteristics determined for jetBL, jetT1 and jetT2 at 60 radii from the nozzle exit from the LES near field by solving the ILEE as described in section III.D are now displayed. The far field of jetT3 has

not been calculated because, due to the close resemblance between the flow fields of jetT2 and jetT3, it is most likely to be very similar to the far field of jetT2. The pressure spectra computed at the angles $\phi = 40^o$ and 90^o relative to the jet direction are represented in figures 14(a-b) as a function of the Strouhal number St_D. Overall, it appears that for both angles and for all frequencies, the noise levels from the two jets with transitional nozzle-exit boundary layers are roughly the same, and that they are lower by about 2 dB than those from the jet with a laminar boundary layer.

In the far-field spectra of jetBL, three additional contributions can be identified: one for $0.15 \leq \mathrm{St}_D \leq 0.5$ at $\phi = 40^o$ in figure 14(a), and two others respectively for $0.5 \leq \mathrm{St}_D \leq 0.6$ and for $\mathrm{St}_D \geq 1$ at $\phi = 90^o$ in figure 14(b). The first noise increase is observed at low frequencies in the downstream direction, where the subsonic jet noise component associated with the large-scale structures developing near the end of the potential core is known to predominate.[67–70] Therefore, it probably results from the higher turbulence intensities encountered on the jet axis in jetBL, shown in figure 12. As pointed out in the previous section based on a comparison with the experimental data of Raman *et al.*,[6] the difference in centerline fluctuation levels in the present simulations may be due to the relatively thick boundary layers of the jets. The low-frequency extra noise from the jet with an exit laminar velocity profile might thus disappear with thinner boundary layers.

The additional acoustic components obtained for jetBL at $\phi = 90^o$ in the medium frequency range are centered around $\mathrm{St}_D = 0.55$, which is one half of the peak frequency in the velocity spectra at $r = r_0$ and $z = r_0$ presented in figure 9(a). As a result, they may be caused by the pairings of coherent structures downstream of the mixing-layer rolling-up, which constitute major sound sources in fully laminar jets.[13,15,26,29] Such sources seem to be present in jetBL presumably because, with a peak turbulence intensity $u'_e/u_j = 6\%$ at the nozzle exit, the jet is initially only moderately disturbed.

Finally, the excess noise radiated by jetBL at $\phi = 90^o$ for $\mathrm{St}_D \geq 1$ may be produced by the larger velocity fluctuations found downstream of $z \simeq 2r_0$ in the shear layers, see in figure 8. Most of the high-frequency jet noise is indeed generated in this flow region according to source localisation studies.[71–74] A similar excess noise can be noted in the sideline sound spectra measured by Viswanathan & Clark,[19] Zaman[20] and Karon & Ahuja[21] for subsonic jets from ASME and conical nozzles of identical diameter. More noise is emitted in the first case, which was attributed by Zaman[20] to the fact that the exit boundary layers are nominally laminar with the ASME nozzle, but turbulent with the conical nozzle. In support of this, their shape factors, given in Karon & Ahuja[21] for a diameter of 1.5 inches, are systematically lower for the conical nozzle, with for instance H = 2.34 in the ASME case but H = 1.71 in the conical case at a Mach number M = 0.4. The present results consequently suggest that the discrepancy in high-frequency noise between ASME and conical nozzles is at least partially due to the difference in the boundary-layer profile.

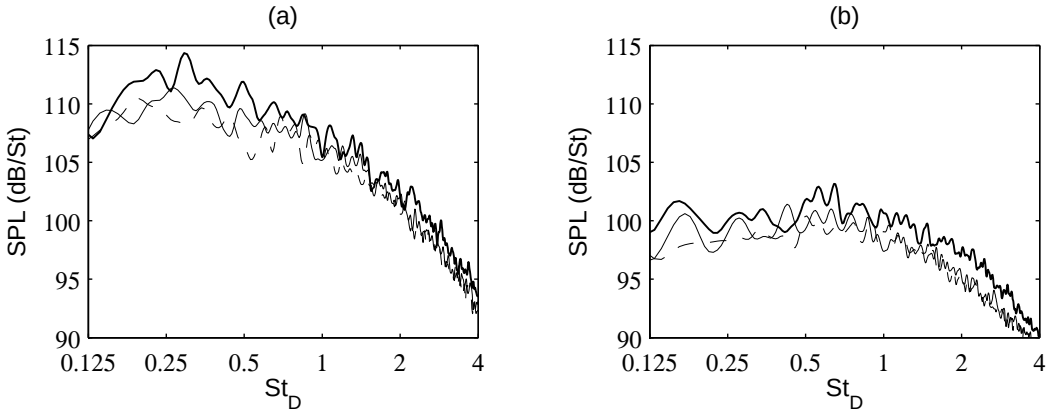

Figure 14. Sound pressure levels (SPL) obtained at a distance of $60r_0$ from the nozzle exit for the angles (a) $\phi = 40^o$ and (b) $\phi = 90^o$ relative to the jet direction, as a function of St_D: ——— jetBL, ——— jetT1, – – – jetT2, – · – · jetT3.

IV. Conclusion

The influence of the initial velocity profile has been investigated using LES for isothermal round jets at a Mach number M = 0.9 and a Reynolds number $\mathrm{Re}_D = 5 \times 10^4$ with nearly identical boundary-layer momentum thicknesses and peak turbulence intensities at the exit of pipe nozzle. One jet with a laminar boundary-layer profile of shape factor H = 2.36, and three jets with transitional profiles and H = 1.68, 1.77 and 2.01, are considered. The results obtained in the transitional cases, whose accuracy is shown by a grid refinement study, are relatively close, but they are significantly different from those from the laminar case. As the velocity profile switches from laminar to turbulent, the peak components in the velocity spectra shift towards higher azimuthal modes at the nozzle exit near the lip, and towards higher frequencies just downstream. The main changes on the flow and acoustic fields are a slower development of the mixing layers with weaker velocity fluctuations, a longer potential core, and lower noise levels in the sideline direction in the medium and high frequency ranges. These changes correspond to those observed when initially laminar jets are tripped and become initially turbulent. Interestingly, they are also similar to those occurring when the amplitude of the exit velocity disturbances increases,[26,29] and when the Reynolds number based on the boundary-layer momentum thickness rises.[30,31] It therefore appears that the effects due to the shape and to the thickness of the exit velocity profile and to the turbulence level at the nozzle exit most often mutually amplify, since initially turbulent jets usually have thicker and sharper boundary-layer profiles and contain stronger upstream fluctuations than initially laminar jets. These effects can however counteract each other in some cases, in particular when initially laminar jets are highly disturbed and exhibit a peak turbulence intensity of about or more than 10% at the nozzle exit.

Appendix A

In jetT1 and jetT2 simulations, the axial velocity profiles T1 and T2 given by equation (2) with $i = 1$ and 2 are imposed at the pipe-nozzle inlet. They have been designed to fit the experimental data obtained by Schubauer & Klebanoff[37] in a boundary layer over a flat plate in the region of laminar-turbulent flow transition. Comparisons between the model profiles and the measurements are presented in figure 15(a-b) using appropriate boundary-layer thicknesses δ_{T1} and δ_{T2}. A very good agreement is observed close to the wall as well as further away.

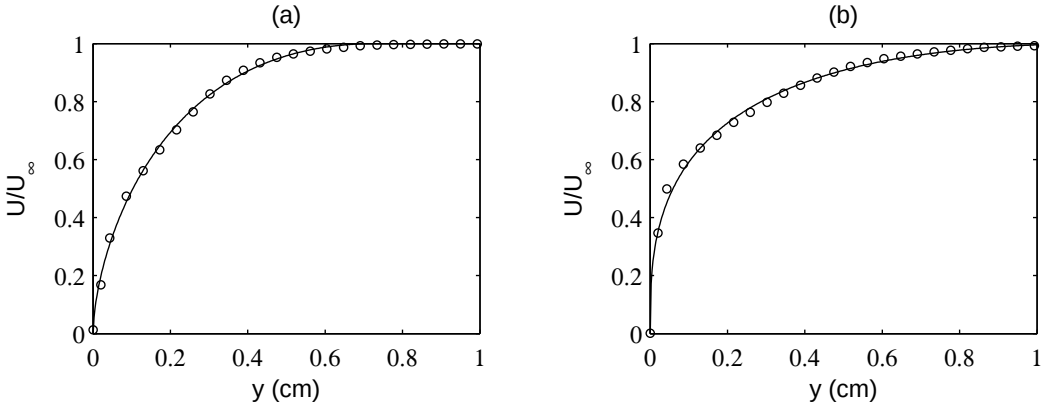

Figure 15. Representation of boundary-layer mean velocity profiles measured by Schubauer & Klebanoff[37] close to the laminar-turbulent transition and of profiles given by equation (2) with $y = r_0 - r$: (a) ∘ measurements at $x = 1.91$ m and ——— profile T1 with $\delta_{T1} = 0.73$ cm, (b) ∘ measurements at $x = 2.06$ m and ——— profile T2 with $\delta_{T2} = 1.17$ cm.

Appendix B

In a preliminary grid convergence study, simulations of jetT1, jetT2 and jetT3 have been performed on a grid finer than the reference grid defined in table 2, limited to $z = 4r_0$ in the axial direction in order to save computational time. The new grid is identical to the other one in the directions θ and z, but differ in the direction r with a mesh spacing $\Delta r/r_0 = 0.18\%$ instead of $\Delta r/r_0 = 0.36\%$ at $r = r_0$. In the additional LES,

the tripping procedure is exactly the same as in the LES using the reference grid, and the time step is twice as small because of the CFL stability condition, leading to an application of the relaxation filtering that is twice as frequent. The flow properties obtained using the two different grids at the nozzle exit and in the mixing layers are found to be very similar. Consequently, they depend neither on the wall-normal spacing, nor on the explicit filtering applied here to remove grid-to-grid oscillations as well as to relax subgrid-scale turbulent energy.

By way of illustration, some results from the simulations of jetT2 are represented, including vorticity snapshots in figure 16(a-b), the radial profiles at the nozzle-exit of mean axial velocity and of turbulence intensities using outer units in figures 17(a-b) and wall units 18(a-b), and the variations of the shear-layer momentum thickness and of the peak turbulence intensities in figures 19(a-b). In the last three figures, the solutions calculated with the reference grid (in black) and with the finer grid (in grey) superpose or are very close to each other.

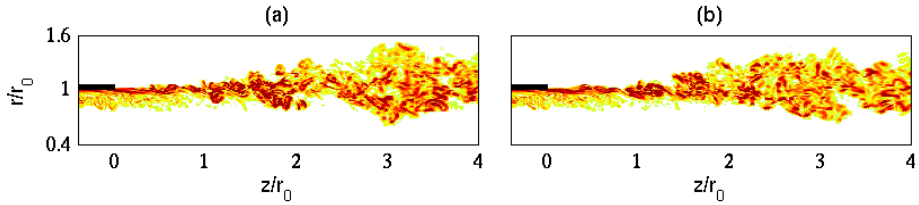

Figure 16. Snapshots in the (z, r) plane of vorticity norm $|\omega|$ obtained for jetT2 using (a) the grid defined in table 2 and (b) a finer grid with $\Delta r/r_0 = 0.18\%$ instead of $\Delta r/r_0 = 0.36\%$ at $r = r_0$. The color scale ranges up to the level of $18u_j/r_0$,

Acknowledgments

This work was granted access to the HPC resources of CINES (Centre Informatique National de l'Enseignement Supérieur) and IDRIS (Institut du Développement et des Ressources en Informatique Scientifique) under the allocation 2013-2a0204 made by GENCI (Grand Equipement National de Calcul Intensif).

References

[1]Crow, S.C. and Champagne, F.H., "Orderly structure in jet turbulence," *J. Fluid Mech.*, Vol. 48, 1971, pp. 547-591.

[2]Hill, W.G., Jenkins, R.C., and Gilbert, B.L., "Effects of the initial boundary-layer state on turbulent jet mixing," *AIAA J.*, Vol. 14, No. 11, 1976, pp. 1513-1514.

[3]Browand, F.K. and Latigo, B.O., "Growth of the two-dimensional mixing layer from a turbulent and nonturbulent boundary layer," *Phys. Fluids*, Vol. 22, No. 6, 1979, pp. 1011-1019.

[4]Hussain, A.K.M.F and Zedan, M.F., "Effects of the initial condition on the axisymmetric free shear layer: Effects of the initial momentum thickness," *Phys. Fluids*, Vol. 21, No. 7, 1978, pp. 1100-1112.

[5]Husain, Z.D. and Hussain, A.K.M.F., "Axisymmetric mixing layer: influence of the initial and boundary conditions," *AIAA J.*, Vol. 17, No. 1, 1979, pp. 48-55.

[6]Raman, G., Zaman, K.B.M.Q., and Rice, E.J., "Initial turbulence effect on jet evolution with and without tonal excitation," *Phys. Fluids A*, Vol. 1, No. 7, 1989, pp. 1240-1248.

[7]Raman, G., Rice, E.J., and Reshotko, E., "Mode spectra of natural disturbances in a circular jet and the effect of acoustic forcing," *Exp. Fluids*, Vol. 17, 1994, pp. 415-426.

[8]Russ, S. and Strykowski, P.J., "Turbulent structure and entrainment in heated jets: The effect of initial conditions," *Phys. Fluids A*, Vol. 5, No. 12, 1993, pp. 3216-3225.

[9]Xu, G. and Antonia, R.A., "Effects of different initial conditions on a turbulent free jet," *Exp. Fluids*, Vol. 33, 2002, pp. 677-683.

[10]Crighton, D.G., "Acoustics as a branch of fluid mechanics," *J. Fluid Mech.*, Vol. 106, 1981, pp. 261-298.

[11]Lilley, G.M., "Jet noise classical theory and experiments," in *Aeroacoustics of Flight Vehicles*, Vol. 1, Noise Sources, Ed. H.H. Hubbard, Acoustical Society of America, 1994, pp. 211289.

[12]Maestrello, L. and McDaid, E., "Acoustic characteristics of a high-subsonic jet," *AIAA J.*, Vol. 9, No. 6, 1971, pp. 1058-1066.

[13]Zaman, K.B.M.Q., "Effect of initial condition on subsonic jet noise," *AIAA J.*, Vol. 23, 1985, pp. 1370-1373.

[14]Zaman, K.B.M.Q., "Far-field noise of a subsonic jet under controlled excitation," *J. Fluid Mech.*, Vol. 152, 1985, pp. 83-111.

[15]Bridges, J.E. and Hussain, A.K.M.F., "Roles of initial conditions and vortex pairing in jet noise," *J. Sound Vib.*, Vol. 117, No. 2, 1987, pp. 289-311.

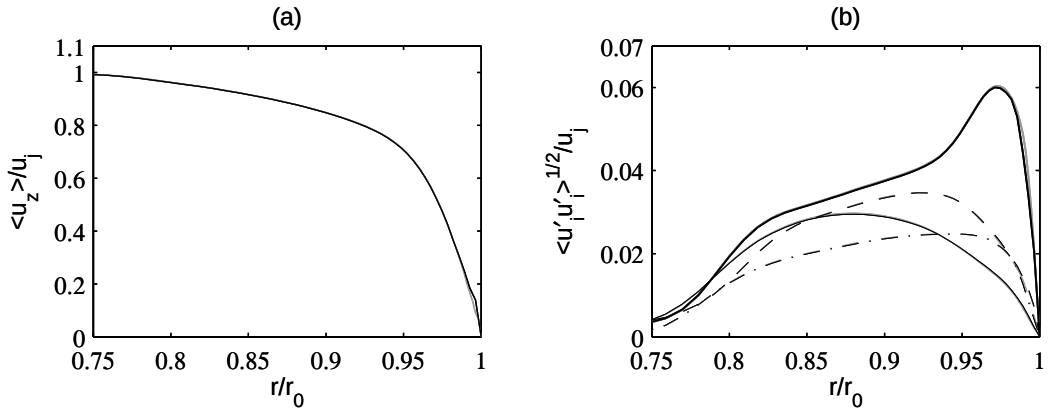

Figure 17. Radial profiles at the nozzle exit (a) of mean axial velocity $< u_z >$ and (b) of turbulence intensities ——— $< u_z'^2 >^{1/2} /u_j$, ——— $< u_r'^2 >^{1/2} /u_j$, – – – $< u_\theta'^2 >^{1/2} /u_j$ and – · – · $< u_r' u_z' >^{1/2} /u_j$ obtained for jetT2 using (black) the reference grid and (grey) the finer grid.

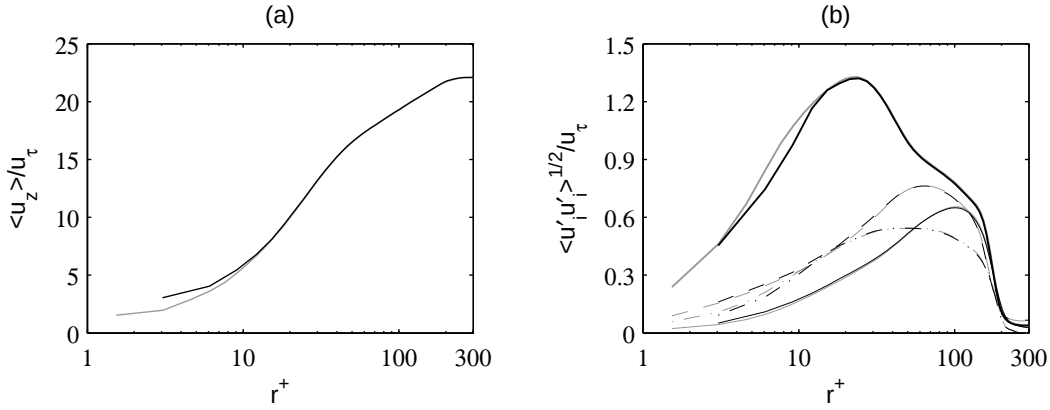

Figure 18. Radial profiles at the nozzle exit (a) of mean axial velocity and (b) of turbulence intensities, represented in wall units based on the wall friction velocity using the same linetypes as in figure 17.

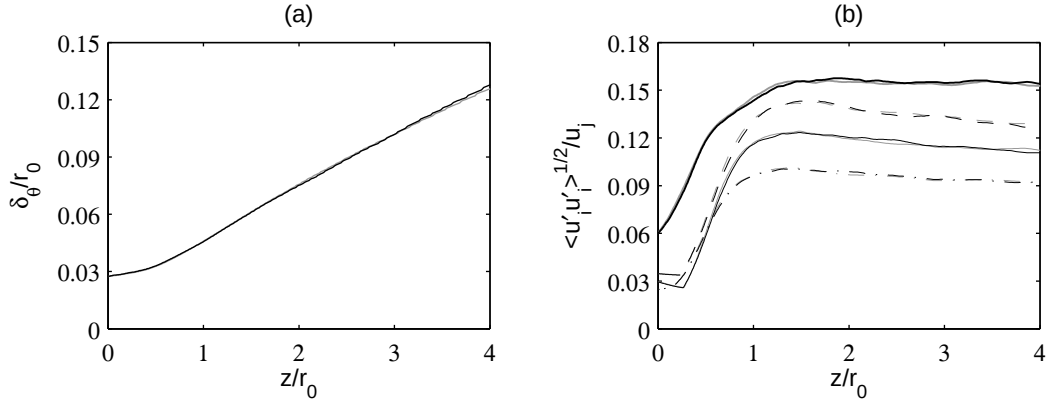

Figure 19. Variations (a) of shear-layer momentum thickness δ_θ and (b) the peak values of turbulence intensities ——— $< u_z'^2 >^{1/2} /u_j$, ——— $< u_r'^2 >^{1/2} /u_j$, – – – $< u_\theta'^2 >^{1/2} /u_j$ and – · – · $< u_r' u_z' >^{1/2} /u_j$ obtained for jetT2 using (black) the reference grid and (grey) the finer grid.

[16]Viswanathan, K., "Aeroacoustics of hot jets," *J. Fluid Mech.*, Vol. 516, 2004, pp. 39-82.

[17]Tanna, H.K., "An experimental study of jet noise. Part I: Turbulent mixing noise," *J. Sound Vib.*, Vol. 50, No. 3, 1977, pp. 405-428.

[18]Harper-Bourne, M., "Jet noise measurements: past and present," *Int. J. of Aeroacoustics*, Vol. 9, No. 4 & 5, 2010, pp. 559-588.

[19]Viswanathan, K. and Clark, L.T., "Effect of nozzle internal contour on jet aeroacoustics," *Int. J. of Aeroacoustics*, Vol. 3, No. 2, 2004, pp. 103-135.

[20]Zaman, K.B.M.Q., "Effect of initial boundary-layer state on subsonic jet noise," *AIAA J.*, Vol. 50, No. 8, 2012, pp. 1784-1795.

[21]Karon, A.Z. and Ahuja, K.K., "Effect of nozzle-exit boundary layer on jet noise," AIAA Paper 2013-0615, 2013.

[22]Zaman, K.B.M.Q., "Effect of initial condition on subsonic jet noise from two rectangular nozzles," AIAA Paper 2012-2160, 2012.

[23]Colonius, T. and Lele, S.K., "Computational aeroacoustics: progress on nonlinear problems of sound generation," *Progress in Aerospace Sciences*, Vol. 40, 2004, pp. 345-416.

[24]Bailly, C. and Bogey, C., "Contributions of CAA to jet noise research and prediction," *Int. J. Comput. Fluid Dyn.*, Vol. 18, No. 6, 2004, pp. 481-491.

[25]Wang, M., Freund, J.B., and Lele, S.K., "Computational prediction of flow-generated sound," *Annu. Rev. Fluid. Mech.*, Vol. 38, 2006, pp. 483-512.

[26]Bogey, C. and Bailly, C., "Influence of nozzle-exit boundary-layer conditions on the flow and acoustic fields of initially laminar jets," *J. Fluid Mech.*, Vol. 663, 2010, pp. 507-539.

[27]Bogey, C., Marsden, O., and Bailly, C., "Large-Eddy Simulation of the flow and acoustic fields of a Reynolds number 10^5 subsonic jet with tripped exit boundary layers," *Phys. Fluids*, Vol. 23, No. 3, 2011, 035104.

[28]Bogey, C., Marsden, O., and Bailly, C., "On the spectra of nozzle-exit velocity disturbances in initially nominally turbulent jets," *Phys. Fluids*, Vol. 23, No. 9, 2011, 091702.

[29]Bogey, C., Marsden, O., and Bailly, C., "Influence of initial turbulence level on the flow and sound fields of a subsonic jet at a diameter-based Reynolds number of 10^5," *J. Fluid Mech.*, Vol. 701, 2012, pp. 352-385.

[30]Bogey, C., Marsden, O., and Bailly, C., "Effects of moderate Reynolds numbers on subsonic round jets with highly disturbed nozzle-exit boundary layers," *Phys. Fluids*, Vol. 24, No. 10, 2012, 105107.

[31]Bogey, C. and Marsden, O., "Identification of the effects of the nozzle-exit boundary-layer thickness and its corresponding Reynolds number in initially highly disturbed subsonic jets," *Phys. Fluids*, Vol. 25, No. 5, 2013, 055106.

[32]Bogey, C., Barré, S., and Bailly, C., "Direct computation of the noise generated by subsonic jets originating from a straight pipe nozzle," *Int. J. Aeroacoust.*, Vol. 7, No. 1, 2008, pp. 1-22.

[33]Uzun, A. and Hussaini, M., "Investigation of high frequency noise generation in the near-nozzle region of a jet using large eddy simulation," *Theoret. Comput. Fluid Dynamics*, Vol. 21, No. 4, 2007, pp. 291-321.

[34]Sandberg, R.D., Sandham, N.D., and Suponitsky, V., "DNS of compressible pipe flow exiting into a coflow," *Int. J. Heat and Fluid Flow*, Vol. 35, 2012, pp. 33-44.

[35]Bühler, S., Kleiser, L. and Bogey, C., "Simulation of subsonic turbulent nozzle-jet flow and its near-field sound," *AIAA J.*, to appear, 2014.

[36]Morris, P.J. and Zaman, K.B.M.Q., "Velocity measurements in jets with application to noise source modelling," *J. Sound Vib.*, Vol. 329, No. 4, 2009, pp. 394-414.

[37]Schubauer, G.B. and Klebanoff, P.S., "Contributions on the mechanics of boundary-layer transition," NACA TN-3498, 1955.

[38]De Chant, L.J., "The venerable 1/7th power law turbulent velocity profile: a classical nonlinear boundary value problem solution and its relationship to stochastic processes," *Appl. Math. Comput.*, Vol. 161, No. 2, 2005, pp. 463-474.

[39]Klebanoff, P.S. and Diehl, Z.W., "Some features of artificially thickened fully developed turbulent boundary layers with zero pressure gradient," NACA TN-1110, 1952.

[40]Coles, D.E., "The turbulent boundary layer in a compressible fluid," Rand. Rep. R-403-PR, 1962.

[41]Erm, P.L. and Joubert, P.N, "Low-Reynolds-number turbulent boundary layers," *J. Fluid Mech.*, Vol. 230, 1991, pp. 1-44.

[42]Schlatter, P and Örlü, R., "Turbulent boundary layers at moderate Reynolds numbers: inflow length and tripping effects," *J. Fluid Mech.*, Vol. 710, 2012, pp. 5-34.

[43]Hutchings, N., "Caution: tripping hazards," *J. Fluid Mech.*, Vol. 710, 2012, pp. 1-4.

[44]Castillo, L. and Johansson, T.G., "The effects of the upstream conditions on a low Reynolds number turbulent boundary layer with zero pressure gradient," *J. Turbulence*, Vol. 3, 2012, 031.

[45]Mohseni, K. and Colonius, T., "Numerical treatment of polar coordinate singularities," *J. Comput. Phys.*, Vol. 157, No. 2, 2000, pp. 787-795.

[46]Bogey, C., de Cacqueray, N., and Bailly, C., "Finite differences for coarse azimuthal discretization and for reduction of effective resolution near origin of cylindrical flow equations," *J. Comput. Phys.*, Vol. 230, No. 4, 2011, pp. 1134-1146.

[47]Bogey, C. and Bailly, C., "A family of low dispersive and low dissipative explicit schemes for flow and noise computations," *J. Comput. Phys.*, Vol. 194, No. 1, 2004, pp. 194-214.

[48]Bogey, C., de Cacqueray, N., and Bailly, C., "A shock-capturing methodology based on adaptative spatial filtering for high-order non-linear computations," *J. Comput. Phys.*, Vol. 228, No. 5, 2009, pp. 1447-1465.

[49]Berland, J., Bogey, C., Marsden, O., and Bailly, C., "High-order, low dispersive and low dissipative explicit schemes for multi-scale and boundary problems," *J. Comput. Phys.*, Vol. 224, No. 2, 2007, pp. 637-662.

[50]Tam, C.K.W and Dong, Z., "Radiation and outflow boundary conditions for direct computation of acoustic and flow disturbances in a nonuniform mean flow., *J. Comput. Acoust.*, Vol. 4, No. 2,, 1996, pp. 175201.

[51]Bogey, C. and Bailly, C., "Three-dimensional non reflective boundary conditions for acoustic simulations: far-field formulation and validation test cases," *Acta Acustica*, Vol. 88, No. 4, 2002, pp. 463-471.

[52]Bogey, C. and Bailly, C., "Large Eddy Simulations of transitional round jets: influence of the Reynolds number on flow development and energy dissipation," *Phys. Fluids*, Vol. 18, No. 6, 2006, 065101.

[53]Bogey, C. and Bailly, C., "Turbulence and energy budget in a self-preserving round jet: direct evaluation using large-eddy simulation," *J. Fluid Mech.*, Vol. 627, 2009, pp. 129-160.

[54]Fauconnier, D., Bogey, C., and Dick, E., "On the performance of relaxation filtering for large-eddy simulation," *J. Turbulence*, Vol. 14, No. 1, 2013, pp. 22-49.

[55]Kremer, F. and Bogey, C., "Large-eddy simulation of turbulent channel flow using relaxation filtering: resolution requirement and Reynolds number effects," submitted to *Comput. Fluids*, 2014. See also AIAA Paper 2013-517.

[56]Kim, J., Moin, P., and Moser, R., "Turbulence statistics in fully developed channel flow at low Reynolds number," *J. Fluid Mech.*, Vol. 177, 1987, pp. 133-166.

[57]Spalart, P.R., "Direct simulation of a turbulent boundary layer up to $R_\theta = 1410$," *J. Fluid Mech.*, Vol. 187, 1988, pp. 61-98.

[58]Gloerfelt, X. and Berland, J., "Turbulent boundary layer noise: direct radiation at Mach number 0.5," *J. Fluid Mech.*, Vol. 723, 2012, pp. 318-351.

[59]Bogey, C., Barré, S., Juvé, D., and Bailly, C., "Simulation of a hot coaxial jet : direct noise prediction and flow-acoustics correlations," *Phys. Fluids*, Vol. 21, No. 3, 2009, 035105.

[60]Ahuja, K.K., Tester, B.J., and Tanna, H.K., "Calculation of far field jet noise spectra from near field measurements with true source location," *J. Sound Vib.*, Vol. 116, No. 3, 1987, pp. 415-426.

[61]Fernholz, H.H. and Finley, P.J., "The incompressible zero-pressure-gradient turbulent boundary layer: an assessment of the data," *Prog. Aerospace Sci.*, Vol. 32, No. 4, 1996, pp. 245-311.

[62]Tomkins, C.D. and Adrian, R.J., "Energetic spanwise modes in the logarithmic layer of a turbulent boundary layer," *J. Fluid Mech.*, Vol. 545, 2005, pp. 141-162.

[63]Brown, G.L. and Roshko, A., "On density effects and large structure in turbulent mixing layers," *J. Fluid Mech.*, Vol. 64, No. 4, 1974, pp. 775816.

[64]Hussain, A.K.M.F. and Zedan, M.F., "Effects of the initial condition on the axisymmetric free shear layer: Effects of the initial fluctuation level," *Phys. Fluids*, Vol. 21, No. 9, 1978, pp. 1475-1481.

[65]Michalke, A., "Survey on jet instability theory," *Prog. Aerospace Sci.*, Vol. 21, 1984, pp. 159-199.

[66]Gutmark, E. and Ho, C.-M., "Preferred modes and the spreading rates of jets," *Phys. Fluids*, Vol. 26, No. 10, 1983, pp. 2932-2938.

[67]Tam, C.K.W., "Jet noise: since 1952," *Theoret. Comput. Fluid Dynamics*, Vol. 10, 1998, pp. 393-405.

[68]Panda, J., Seasholtz, R.G., and Elam, K.A., "Investigation of noise sources in high-speed jets via correlation measurements," *J. Fluid Mech.*, Vol. 537, 2005, pp. 349-385.

[69]Bogey, C. and Bailly, C., "An analysis of the correlations between the turbulent flow and the sound pressure field of subsonic jets," *J. Fluid Mech.*, Vol. 583, 2007, pp. 71-97.

[70]Tam, C.K.W., Viswanathan, K., Ahuja, K.K., and Panda, J., "The sources of jet noise: experimental evidence," *J. Fluid Mech.*, Vol. 615, 2008, p. 253-292.

[71]Chu, W.T. and Kaplan, R.E., "Use of a spherical concave reflector for jet-noise-source distribution diagnosis," *J. Acoust. Soc. Am.*, Vol. 59, No. 6, 1976, pp. 1268-1277.

[72]Fisher, M.J., Harper-Bourne, M., and Glegg, S.A.L., "Jet engine noise source location: The polar correlation technique," *J. Sound Vib.*, Vol. 51, No. 1, 1977, pp. 23-54.

[73]Narayanan, S., Barber, T.J. and Polak, D.R., "High subsonic jet experiments: Turbulence and noise generation studies," *AIAA J.*, Vol. 40, No. 3, 2002, pp. 430-437.

[74]Lee, S.S. and Bridges, J., "Phased-array measurements of single flow hot jets," NASA/TM 2005-213826, 2005. See also AIAA Paper 2005-2842.